J. Fluid Mech. (2003), *vol.* 485, *pp.* 87–96.
DOI: 10.1017/S0022112003004439 Printed in the United Kingdom

Dynamics of large-scale structures in turbulent flow over a wavy wall

By NILS KRUSE[1], AXEL GÜNTHER[2] AND PHILIPP RUDOLF VON ROHR[1]†

[1]Institute of Process Engineering, Swiss Federal Institute of Technology (ETH) Zurich, CH-8092 Zurich, Switzerland

[2]Department of Chemical Engineering, Massachusetts Institute of Technology, Cambridge, MA 02139, USA

(Received 12 November 2002 and in revised form 10 March 2003)

We describe the dynamics of large-scale structures in a developed turbulent flow between a train of waves and a flat wall. A water channel facility, for which the wavelength, Λ, of the bottom wall equals the channel height and the wave amplitude is ten times smaller, is used. The channel is sufficiently wide so that structures of spanwise scale $O\{1.5\Lambda\}$ meander laterally. The paper dicusses the temporal behaviour and the meandering motion at a Reynolds number of 4500, defined with the half channel height and the bulk velocity. Digital particle image velocimetry is performed in a horizontal plane with a field of view of $2.6\Lambda \times 2.7\Lambda$. Ten ensembles of 90 consecutive image pairs are acquired at a rate of 15 Hz, a temporal resolution sufficient to assess how the largest flow scales evolve in time. The streamwise velocity $u(x, z, t)$ is filtered using the dominant eigenfunctions that are obtained by a proper orthogonal decomposition analysis. The very large temporal scales of the meandering motion of the $O\{1.5\Lambda\}$ structures could be followed over measurement times of up to 6 s, during which they are convected downstream by distance of 65 wavelengths. The observed coherent lengths in the streamwise direction are significantly larger than the streamwise domain extent of all large-eddy simulation and direct numerical simulation reported so far.

1. Introduction

Longitudinal structures play an important role in a number of transport processes. A wavy bottom wall adds a defined degree of complexity to the turbulent flow between two horizontal walls (e.g. Niederschulte, Adrian & Hanratty 1990; Günther *et al.* 1998). The mean quantities of the flow vary periodically in the streamwise direction and its boundary conditions are well defined. Since moderate Reynolds numbers are considered, direct numerical simulation (DNS) are capable of resolving the smallest scales of the flows. Since the computational domain of the present DNS is of the same order as the 1.5Λ scales, laboratory measurements rather than computational studies seem advantageous to address the dynamics of these large scales.

Early works have described the non-separated, isothermal flow over small-amplitude waves using linear stability analysis. With increasing α, linear analysis eventually becomes insufficient. Following the original contributions of Motzfeld (1937), Miles

† Author to whom correspondence should be addressed: vonrohr@ivuk.mavt.ethz.ch

(1957), Benjamin (1959), and Hanratty and co-workers (e.g. Buckles, Hanratty & Adrian 1984; Hudson, Dykhno & Hanratty 1996), a number of laboratory and numerical experiments were conducted to describe the mean and turbulence quantities of the flow, and turbulence production. The literature on the stability of an isothermal, sheared flow over rigid waves suggests that the Görtler (Görtler 1940; Saric 1994) and the Craik–Leibovich type 2 (CL-2) instability (Phillips & Wu 1994) produces, or catalyses, spanwise-periodic longitudinal vortices. Even though such structures are of three-dimensional nature, the mostly qualitative visualizations have so far been restricted to observations in the (x, y)-plane. Only recently was attention drawn to the effect of the wavy wall with respect to three-dimensional, large-scale structures. Gong, Taylor & Dörnbrack (1996) and Miller (1995) showed the presence of a CL-2 mechanism from a spanwise variation of the mean streamwise velocity in a low-aspect-ratio wind tunnel. Günther & Rudolf von Rohr (2002, 2003) addressed the existence of $O\{1.5\Lambda\}$ scales in a wide channel. In (x, z)-planes above the wave crests the perturbations in the velocity field were found to be the largest, a reason why we consider the same vertical position in this paper. Due to the wavyness of the bottom wall, the mean flow is weakly inhomogeneous in the x-direction in this plane, whereas the spanwise direction, z, can be considered homogeneous at the measurement location in the channel centre. At turbulent conditions and a position $y/\Lambda = 0.26$, the observed longitudinal structures do not have fixed spanwise locations but they meander laterally. A discussion of characteristic scales was based on a proper orthogonal decomposition (POD) analysis of the streamwise velocity component. The dominance of eigenvalues $\lambda_{1,2}$ is limited to the lower half of the channel and increases for increasing Re_h. Scale $\Lambda_z = O\{1.5\Lambda\}$ agrees with that reported by Gong *et al.* (1996). It was concluded that the non-developed flow does not contain the structures we observe for the developed flow situation, but they develop and grow when passing a periodic train of waves in the streamwise direction.

The paper is organized as follows: § 2 describes the experimental facility, and § 3 presents results on the dynamics of the lateral motion of the observed $O\{1.5\Lambda\}$ scales.

2. Experimental

Measurements are carried out in a channel facility. The flow loop is designed for low-Reynolds-number turbulence measurements with light sheet techniques. It contains approximately 0.280 m^3 of de-ionized and filtered water. The entire facility is made of black anodized aluminium, PVC, and Schott BK-7 glass. For a detailed description refer to Günther (2001) or Günther & Rudolf von Rohr (2003).

The full height of the channel, H, is 30 mm and the channel width, B, is $12H$. The wavelength Λ of the sinusoidal wall profile is equal to the channel height. Figure 1 shows the coordinate system and schematically illustrates characteristic regions of the mean flow field in the vicinity of the wavy surface. Coordinate x is directed parallel to the mean flow, y is perpendicular to the top wall, and z is the spanwise coordinate. The corresponding velocity components are denoted u, v, and w. A separation zone (1), bounded by the isosurface of the mean streamfunction $\Psi(x, y) = 0$, is located in the wave troughs. On the uphill side, two regions of maximum (2) and minimum (3) Reynolds shear stress, $-\varrho\overline{u'v'}$, are found. From the DNS results of Cherukat, Hanratty & McLaughin (1998) for $Re_h = 3460$, regions (2) and (3) are found approximately 0.08Λ and 0.01Λ above the wall on the uphill side. The data of Cherukat *et al.* (1998) and Henn & Sykes (1999) identify the energy of traverse velocity fluctuations, $\varrho\overline{w'^2}$, to be maximal at a location that is close to region (3). The developed flow between

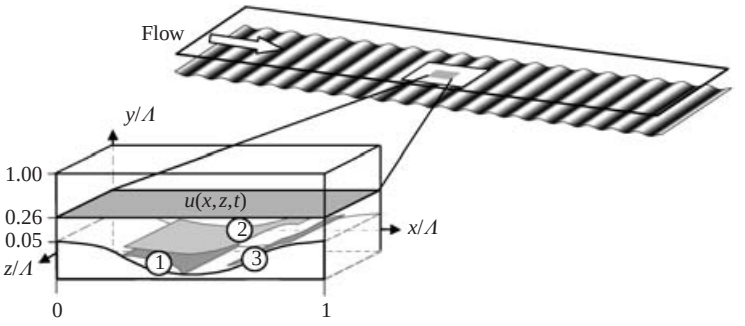

FIGURE 1. Coordinate system and schematic of (1) the separation region, and the regions (2) of maximum positive and (3) negative Reynolds shear stress.

the bottom wall and the bulk is characterized by the ratio of the amplitude, $2a$, to the wavelength, $\alpha = 2a/\Lambda = 0.1$, and the Reynolds number

$$Re_h = \frac{U_b h}{\nu} = 4500, \tag{2.1}$$

where ν denotes the kinematic viscosity, and h is the half-height of the channel. The bulk velocity U_b is defined as

$$U_b = \frac{1}{2h}\int_{y_w}^{2h} U(x_\xi, y)\,\mathrm{d}y = 0.301\ \mathrm{m\,s^{-1}}, \tag{2.2}$$

where x_ξ denotes an arbitrary x-location and $y_w(x) = 0.05\Lambda\cos(x2\pi/\Lambda)$ describes the profile of the wavy surface. Reynolds averaging is used to decompose the velocity into a mean and a fluctuating part: $u = \overline{u} + u'$.

Optical access is provided at four streamwise locations in the wavy channel section through viewing ports at both sidewalls and at the flat top wall. Measurements are performed for a hydrodynamically developed flow after the 50th wave crest. The maxiumum field of view (FOV) for the top windows is 3.3Λ(streamwise) $\times$ 3.3Λ(spanwise). To determine the fluid viscosity, the water temperature is monitored downstream of the test section. We use digital particle image velocimetry (PIV) (Adrian 1991; Westerweel 1995; Raffel, Willert & Kompenhans 1998) to assess the temporal behaviour of large-scale structures in the velocity field. For the velocity measurements with an large FOV of $2.6\Lambda \times 2.7\Lambda$, the flow is seeded with 100 µm polyamide particles (density: 1.01 g cm^{-3}). The measurement system consisting of the laser, the laser optics, and the camera, is positioned on a traverse that allows the vertical position to be changed. The accuracy of adjusting the y-position is approximately 10 µm. A flashlamp-pumped dual Nd:YAG laser provides the pulse light source. An 8-bit CCD camera with a pixel-resolution of 1008×1018 pixels^2 is used for the velocity measurements. Measurements are taken in the (x, z)-plane at $y/H = 0.26$.

3. Results

Instantaneous velocity fields

Measurements in the (x, z)-plane are expected to reveal information that is related to large-scale, longitudinal flow structures. The left-hand column of figure 2 shows a sequence of six contour plots of the instantaneous streamwise velocity in the

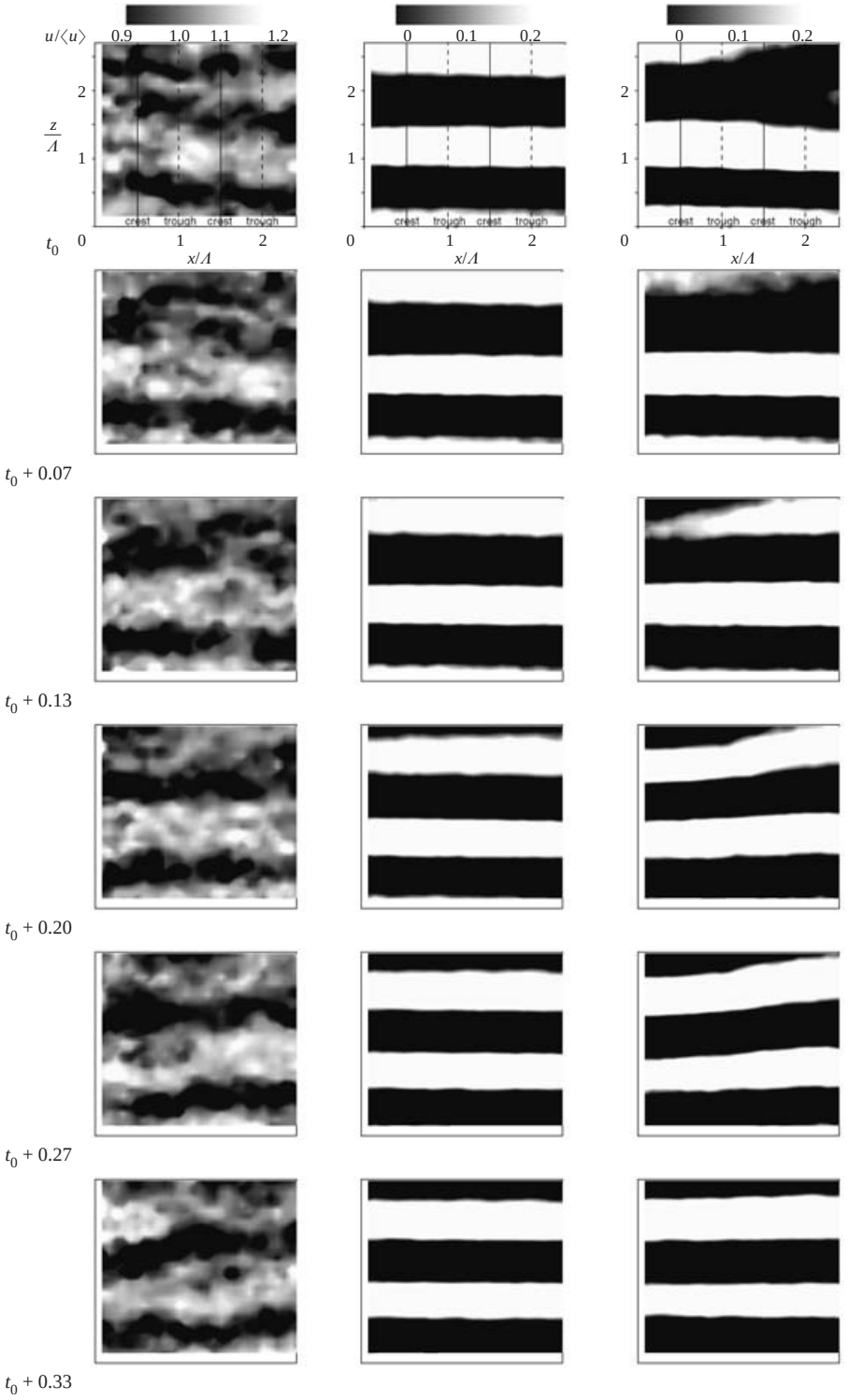

FIGURE 2. Sequence of instantaneous velocities $u(x, y/\Lambda = 0.26, z, t)/\langle u \rangle$ with a temporal separation of $\Delta t = 0.067$ s. Raw data (left-hand column), projection of the first two (centre) and the first eight (right) eigenfunctions on the instantaneous velocity with FOV $= 2.6\Lambda \times 2.7\Lambda$, $Re_h = 4500$. Solid vertical lines denote crested and dashed vertical lines troughs.

(x, z)-plane acquired with a frame rate of 15 Hz. The images correspond to a Reynolds number of 4500. The perturbations in the streamwise velocity were previously found to be the largest at $y/H = 0.26$ (Günther 2001). Due to the waviness of the bottom wall, the mean flow is weakly inhomogeneous in the x-direction in this plane, where the spanwise direction, z, can be considered homogeneous at the measurement location in the channel centre. From the instantaneous plots, the existence of large-scale longitudinal structures is obvious. Large fluid columns with a characteristic distance of $O\{1.5\Lambda\}$ in the spanwise direction can be observed. However, the quantitative contributions of the different scales, or the dominant scale cannot be found by such means. The longitudinal structures observed do not have fixed spanwise locations but they meander laterally. To address the qualitative contribution of the different scales, we now perform a POD analysis with an ensemble of $M = 900$ realizations of the velocity $u(x, y + 0.26\Lambda, z, t)$. The ensemble contains 10 sequences of 90 consecutive velocity fields that were aquired at 15 Hz.

POD analysis

We use the method of snapshots (Sirovich 1987) and perform a Karhunen–Loève (KL) transformation or proper orthogonal decomposition (POD) of the streamwise velocity component (Liu, Adrian & Hanratty 2001; Berkooz, Holmes & Lumley 1993). We consider discrete times t_i with $i = 1, \ldots, M$, and $1, \ldots, N$ discrete locations within the (x, z)-plane, where $N = mn$ with $x : (1, m)$ and $z : (1, n)$. The resulting set of spatio-temporal data can be written as the $N \times M$ matrix:

$$\boldsymbol{U} = \{\boldsymbol{U}_i\}_{i=1}^{M} = \begin{bmatrix} u_{11}, u_{12}, \ldots, u_{1M} \\ u_{21}, u_{22}, \ldots, u_{2M} \\ \vdots \\ u_{N1}, u_{N2}, \ldots, u_{NM} \end{bmatrix} \tag{3.1}$$

with $\boldsymbol{U}_i = [u_1, u_2, \ldots, u_N]^T$. We obtain the mean streamwise velocity by averaging over the columns:

$$\overline{\boldsymbol{U}} = \frac{1}{M} \sum_{i=1}^{M} \boldsymbol{U}_i. \tag{3.2}$$

For the velocity fluctuations it then follow that

$$\boldsymbol{U}_i' = \boldsymbol{U}_i - \overline{\boldsymbol{U}}, \qquad i = 1, \ldots, M. \tag{3.3}$$

Using the method of snapshots, the $M \times M$ covariance matrix becomes

$$\boldsymbol{C}_{ij} = \langle \boldsymbol{U}_i' \boldsymbol{U}_j' \rangle, \qquad i, j = 1, \ldots, M, \tag{3.4}$$

where $\langle \cdot, \cdot \rangle$ is the Euclidean inner product. Since the matrix is symmetric its eigenvalues, λ_i, are non-negative, and its eigenvectors, ϕ_i, $i = 1, \ldots, M$, form a complete orthogonal set. The orthogonal eigenfunctions are:

$$\Pi^{[k]} = \sum_{i=1}^{M} \phi_i^{[k]} \boldsymbol{U}_i', \qquad k = 1, \ldots, M, \tag{3.5}$$

where $\phi_i^{[k]}$ is the ith component of the kth eigenvector. Figure 3 shows the eigenfunctions that correspond to modes 1–8. The results suggest that, for the considered Reynolds numbers, the eigenfunctions Π_1 and Π_2 have a characteristic scale $\Lambda_z = O\{1.5\Lambda\}$ in the spanwise direction.

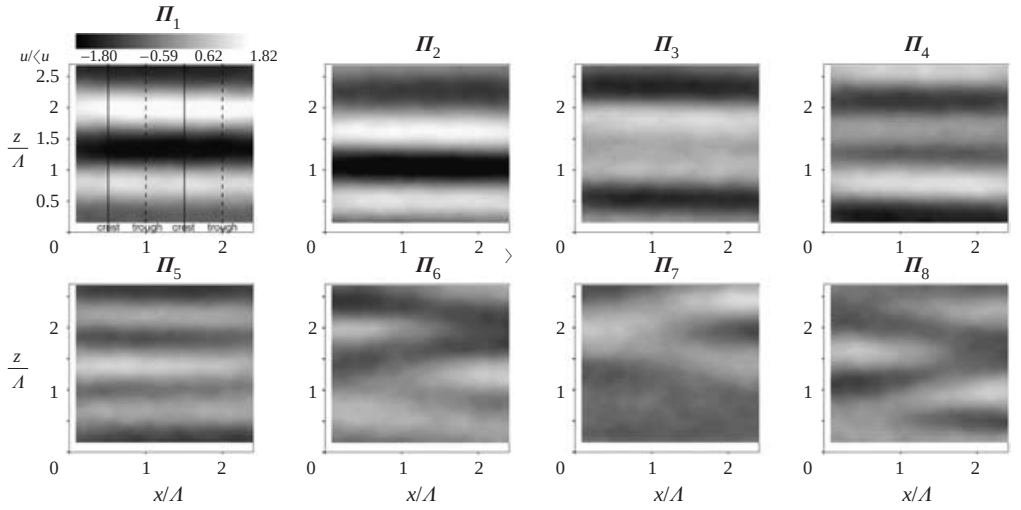

FIGURE 3. Eigenfunctions of modes 1–8 from a decomposition of $u(x, y/\Lambda = 0.26, z, t)$ with FOV $= 2.6\Lambda \times 2.7\Lambda$, $Re_h = 4500$.

We can associate an energy with the velocity fluctuations and obtain, due to the orthogonality of the eigenfunctions (Sirovich 1987; Berkooz *et al.* 1993),

$$E = \sum_{i=1}^{M} \lambda_i. \tag{3.6}$$

The fractional contribution of one eigenfunction's associated eigenvalue is

$$\frac{E_k}{E} = \frac{\lambda_k}{E}. \tag{3.7}$$

Since the mean streamwise velocity is constant in the spanwise direction, note that the POD analysis is identical to a Fourier decomposition in this direction. However, this is not strictly true in the weakly inhomogeneous x-direction, where a POD analysis is the correct way of decomposing the velocity field. Figure 4 shows the eigenvalues $\lambda_1, \ldots, \lambda_{95}$ ranked in decreasing order of their fractional contribution to the turbulent kinetic energy E and confirms the dominance of POD-modes 1 and 2 with a cumulative contribution of $0.25E$.

Temporal evolution

We now have a closer look at the ten sequences of 90 consecutive image pairs (frame rate 15 Hz) that are contained in the ensemble that we used for the POD analysis. Since the FOV is rather large, $2.6\Lambda \times 2.7\Lambda$, the time-resolution of the camera is sufficient to assess the largest flow scales evolving in time. Using only the first K most energetic eigenfunctions, the original data can be approximated as

$$\boldsymbol{U}'_j \doteq \overline{\boldsymbol{U}} + \sum_{i=1}^{K} a_i \Pi^{[i]}, \tag{3.8}$$

where the coefficients a_i are computed from the projection of the sample vector $\boldsymbol{U}'_j$ ($N \times 1$ matrix) onto eigenfunction $\Pi^{[i]}$:

$$a_i = \frac{\boldsymbol{U}'_j \cdot \Pi^{[i]}}{\Pi^{[i]} \cdot \Pi^{[i]}}. \tag{3.9}$$

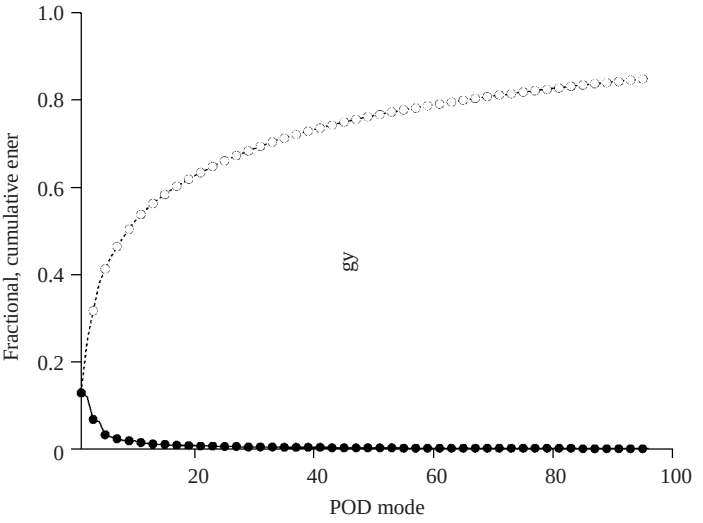

FIGURE 4. Fractional and cumulative contribution from eigenvalues 1–95 obtained for a POD decomposition of $u(x, y/\Lambda = 0.26, z, t)$ with FOV $= 2.6\Lambda \times 2.7\Lambda$, $Re_h = 4500$.

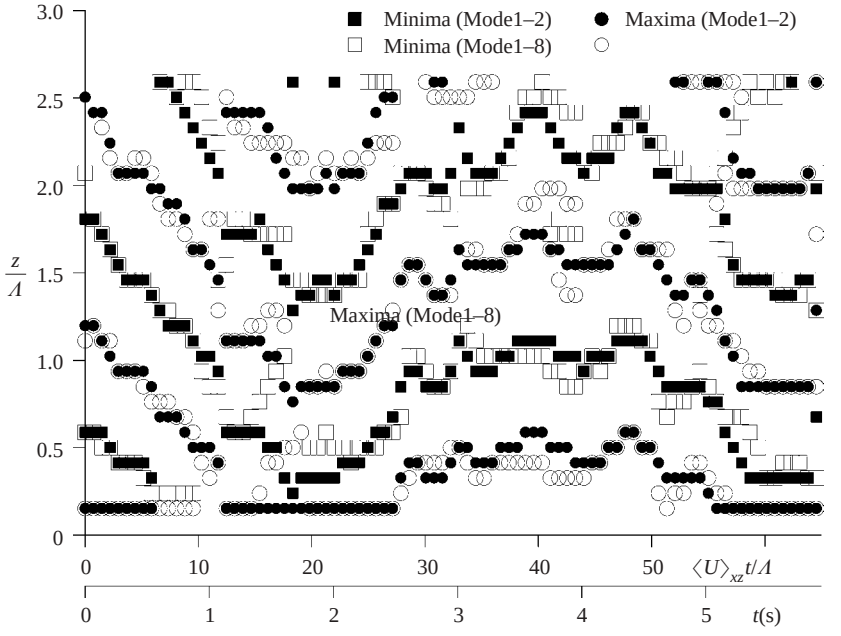

FIGURE 5. Temporal behaviour of velocity minima and maxima detected from instantaneous velocity fields $u(x, y/\Lambda = 0.26, z, t)$ that are reconstructed from (*a*) POD modes 1–2 and (*b*) modes 1–8. FOV $= 2.6\Lambda \times 2.7\Lambda$, $Re_h = 4500$, $\langle U \rangle_{xz} = 0.325\,\mathrm{m\,s^{-1}}$, $U_b = 0.301\,\mathrm{m\,s^{-1}}$.

This operation corresponds to low-pass filtering and is used to study the temporal behaviour of the largest scales. Representative samples of the raw and the corresponding filtered velocity fields are shown in figure 2. Six snapshots of instantaneous velocity fluctuations with a temporal separation of 0.067 s are projected onto eigenmodes 1–2 and 1–8 (containing 25% and 49% of the total energy). The longitudinal structures in figure 2 meander laterally.

Reference	Description of investigation
Maas & Schumann (1994)	$Re_h = 6760$, $x/\Lambda = 4$, $z/\Lambda = 2$, DNS
De Angelis *et al.* (1997)	$x/\Lambda = 6$, $z/\Lambda = 1$, DNS
Cherukat *et al.* (1998)	$Re_h = 3460$, $x/\Lambda = 4$, $z/\Lambda = 2$, DNS
Henn & Sykes (1999)	$Re_h = 6560$–20060, $x/\Lambda = 2$, $z/\Lambda = 1$, LES
Boersma (2000)	$Re_h = 1750$, $x/\Lambda = 5$, $z/\Lambda = 3$, DNS
Calhoun & Street (2001); Calhoun *et al.* (2001)	$Re_h = 7000$, $x/\Lambda = 4$, $z/\Lambda = 2$, LES

TABLE 1. Selected numerical simulations.

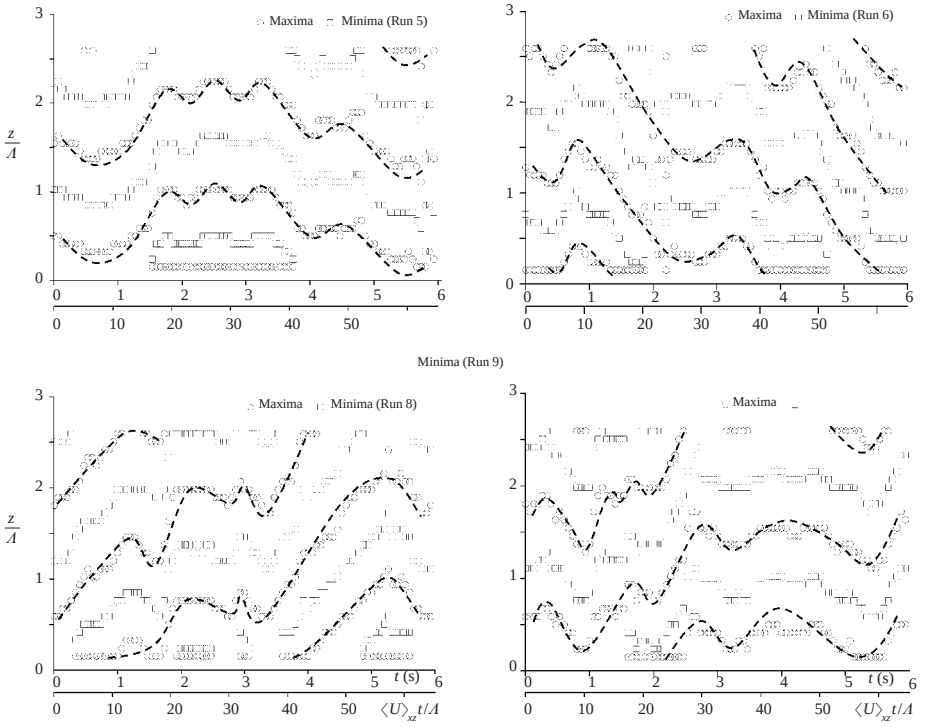

FIGURE 6. Temporal behaviour of velocity minima and maxima for four sequences of 90 velocity fields $u(x, y/\Lambda = 0.26, z, t)$ that are reconstructed from POD modes 1–2. FOV $= 2.6\Lambda \times 2.7\Lambda$, $Re_h = 4500$, $\langle U \rangle_{xz} = 0.325\,\mathrm{m\,s^{-1}}$, $U_b = 0.301\,\mathrm{m\,s^{-1}}$.

For one of the ten sequences figure 5 shows the temporal behaviour of the spanwise maximum/minimum locations of the streamwise-averaged velocity field. Eigenfunctions Π_{1-2} and Π_{1-8} are used for the reconstruction. The total length of the sequence is 6 s. In order to estimate the extent of the $O\{1.5\Lambda\}$ scales in the streamwise direction, we use Taylor's hypothesis and introduce a second abscissa:

$$\hat{x} = t\frac{\langle U \rangle_{xz}}{\Lambda}, \tag{3.10}$$

where $\langle U \rangle_{xz}$ denotes a spatial average of the streamwise mean velocity in the (x, z)-plane.

Projecting onto the first two compared to the first eight modes has no qualitative effect and relatively little quantitative effect on detecting the spanwise location of the extrema in $u(x, y + 0.26\Lambda, z, t)$. We therefore decided to filter the instantaneous velocity fields acquired at 15 Hz by projecting them onto eigenfunctions Π_{1-2} and follow the lateral motion of the corresponding $O\{1.5\Lambda\}$ scales in time. The observed temporal scales of the meandering motion are of the order of seconds, during which they are convected downstream over several tens of wavelengths. The observed large coherence lengths are important for computational studies of the dynamics of the $O\{1.5\Lambda\}$ scales, since the required streamwise extent of the computational domain seems to exceed the capabilities of current DNS and LES (large-eddy simulation) (table 1).

Figure 6 shows the temporal evolution of the obtained maximum and minimum locations for four sequences of 90 velocity fields. Note that the extrema travel more than 2Λ in the spanwise direction during the measuring time of 6 s, corresponding to a streamwise distance of 65Λ.

4. Concluding remarks

The dynamics of large-scale flow structures with a characteristic scale of $O\{1.5\Lambda\}$ in the spanwise direction studied at $Re_h = 4500$ are identified from spatially resolving measurements in the (x, z)-plane. The meandering motion of these scales could be followed over measurement times of up to 6 s, during which they are convected downstream by a distance of 65 wavelengths. The very large coherent lengths observed in the streamwise direction are significantly larger than the streamwise domain extent of all LES and DNS conducted so far. The meandering motion of the $O\{1.5\Lambda\}$-scales provides a mechanism for momentum or scalar transport between the wavy wall and the bulk fluid.

We gratefully acknowledge financial support from the Swiss National Science Foundation (SNF). Measurement technology is partially provided by TSI.

REFERENCES

Adrian, R. J. 1991 Particle-imaging techniques for experimental fluid mechanics. *Annu. Rev. Fluid Mech.* **23**, 261–304.

Benjamin, B. 1959 Shearing flow over wavy boundary. *J. Fluid Mech.* **6**, 161–205.

Berkooz, G., Holmes, P. & Lumley, J. L. 1993 The proper orthogonal decomposition in the analysis of turbulent flows. *Annu. Rev. Fluid Mech.* **25**, 539–575.

Boersma, B. J. 2000 Particle distributions in the flow over a wavy wall. *Proc. Summer School*. Center for Turbulence Res. (CTR). Stanford University/CA.

Buckles, J, Hanratty, T. J. & Adrian, R. J. 1984 Turbulent flow over large-amplitude wavy surfaces. *J. Fluid Mech.* **140**, 27–44.

Calhoun, R. J. & Street, R. L. 2001 Turbulent flow over a wavy surface: Neutral case. *J. Geophys. Res.* **106**, 9277–9293.

Calhoun, R. J., Street, R. L. & Koseff, J. R. 2001 Turbulent flow over a wavy surface: Stratified case. *J. Geophys. Res.* **106**, 9295–9310.

Cherukat, P, Na, Y., Hanratty, T. J. & McLaughlin, J. B. 1998 Direct numerical simulation of a fully developed turbulent flow over a wavy wall. *Theor. Comput. Fluid Dyn.* **11** (2), 109–134.

De Angelis, V., Lombardi, P. & Banerjee, S. 1997 Direct numerical simulation of turbulent flow over a wavy wall. *Phys. Fluids* **3**, 2429–2442.

Gong, W., Taylor, P. A. & Dörnbrack, A. 1996 Turbulent boundary-layer flow over fixed aerodynamically rough two-dimensional sinusoidal waves. *J. Fluid Mech.* **312**, 1–37.

Görtler, H. 1940 Ueber eine dreidimensionale Instabilität laminarer Grenzschichten an konkaven Wänden. *Nachr. Ges. Wiss. Göttingen, Math-Phys. Klasse, Neue Folge I*, **2**, 1–26.

Günther, A. 2001 Large-scale structures in Rayleigh-Bénard convection and flow over waves. PhD thesis, ETH Zurich, Switzerland, Diss. ETH 14359.

Günther, A., Papavassiliou, D. V., Warholic, M. D. & Hanratty, T. J. 1998 Turbulent flow in a channel at a low Reynolds number. *Exps. Fluids* **25**, 503–511.

Günther, A. & Rudolf von Rohr, Ph. 2002 Structure of the temperature field for flow over heated waves. *Exps. Fluids* **33**, 920–930.

Günther, A. & Rudolf von Rohr, Ph. 2003 Large scale structures in a developed flow over a wavy wall. *J. Fluid Mech.* **478**, 257–285.

Henn, D. S. & Sykes, R. I. 1999 Larges-eddy simulation of flow over wavy surfaces. *J. Fluid Mech.* **383**, 75–112.

Hudson, J. D., Dykhno, L. & Hanratty, T. J. 1996 Turbulence production in flow over a wavy wall. *Exps. Fluids* **20**, 257–265.

Liu, Z.-C., Adrian, R. J. & Hanratty, T. J. 2001 Large-scale modes of turbulent channel flow: transport and structure. *J. Fluid Mech.* **448**, 53–80.

Mass, C. & Schumann, U. 1996 Direct numerical simulation of separated turbulent flow over a wavy boundary. In *Flow Simulation with High Performance Computers* (ed. E. H. Hirschel); Notes on Numerical Fluid Mechanics, vol. 52, pp. 227–241, see ER-COFTAC database, http://fluindigo.mech.surrey.ac.uk/database/test77/test77.html

Miles, J. 1957 On the generation of surface waves by shear flows. *J. Fluid Mech.* **3**, 185–204.

Miller, C. A. 1995 Turbulent boundary layer above complex terrain. PhD thesis, University of Western Otario, Canada.

Motzfeld, H. 1937 Die turbulente Strömung an welligen Wänden. *Z. Angew. Math. Mech.* **47**, 193–212.

Niederschulte, M. A., Adrian, R. J. & Hanratty, T. J. 1990 Measurements of turbulent flow in a channel at low Reynolds numbers. *Exps. Fluids* **8**, 222–231.

Phillips, W. R. C. & Wu, Z. 1994 On the instability of wave-catalysed longitudinal vortices in strong shear. *J. Fluid Mech.* **272**, 235–254.

Raffel, M., Willert, C. & Kompenhans, J. 1998 *Particle Image Velocimetry. A Practical Guide*. Springer.

Saric, W. S. 1994 Görtler vortices. *Annu. Rev. Fluid Mech.* **26**, 379–409.

Sirovich, L. 1987 Turbulence and the dynamics of coherent structures, Pt I: Coherent structures. *Q. of Appl. Maths.* **XLV**, 561–571.

Sullivan, P. P., McWilliams, J. C. & Moeng, C-H. 2000 Simulation of idealised flow over water waves. *J. Fluid Mech.* **404**, 47–85.

Westerweel, J. 1995 Fundamentals of digital particle image velocimetry. *Meas. Sci. Technol.* **8**, 1379–1392.